Heat Mass Transfer (2011) 47:119–130
DOI 10.1007/s00231-010-0674-7

ORIGINAL

Effects of Knudsen number and geometry on gaseous flow and heat transfer in a constricted microchannel

Hossein Shokouhmand · Sajjad Bigham · Rasool Nasr Isfahani

Received: 15 September 2009 / Accepted: 6 September 2010 / Published online: 21 September 2010

Abstract A flow and heat transfer numerical simulation is performed for a 2D laminar incompressible gas flow through a constricted microchannel in the slip regime with constant wall temperature. The effects of rarefaction, creeping flow, first order slip boundary conditions and hydrodynamically/thermally developing flow are assumed. The effects of Knudsen number and geometry on thermal and hydrodynamic characteristics of flow in a constricted microchannel are explored. SIMPLE algorithm in curvilinear coordinate is used to solve the governing equations including continuity, energy and momentum with the temperature jump and velocity slip conditions at the solid walls in discretized form. The resulting velocity and temperature profiles are then utilized to obtain the microchannel C_f Re and Nusselt number as a function of Knudsen number and geometry. The results show that Knudsen number has declining effect on the C_f Re and Nusselt number in the constricted microchannel. In addition, the temperature jump on wall and slip velocity increase with increasing Knudsen number. Moreover, by decreasing the throttle area, the fluid flow characteristics experience more intense variations in the constricted region. To verify the code a comparison is carried out with available results and good agreement is achieved.

List of symbols

a	Amplitude of the wave (m)
k	Thermal conductivity of air (W/m K)
h	Local heat transfer coefficient (W/m^2 K)
J	Jacobian of the coordinate transformation
p	Dimensionless pressure
Re	Reynolds number (Re $= \rho u_i L^*/\mu$)
Pr	Prandtl number ($Pr = \nu/\alpha$)
Nu	Local Nusselt number
Nu_∞	Fully developed Nusselt number
Kn	Knudsen number
Ma	Mach number
Pe	Peclet number
Ec	Eckert number
C_f	Skin-friction coefficient
c_p	Specific heat (J/kg K)
n	Dimensionless normal direction to the wall
s	Dimensionless tangential direction to the wall
q_{11}, q_{22}, q_{12}	Grid parameters
R	Gas constant (J/kg K)
T	Temperature (K)
q''	Heat flux
u	Dimensionless velocity component in x-direction
v	Dimensionless velocity component in y-direction
L^*	Channel inlet width
x	Dimensionless horizontal coordinate
y	Dimensionless vertical coordinate

Greek symbols

α	Thermal diffusivity (m^2/s)
λ	Surface wavelength (m)
ρ	Density of fluid (kg/m^3)
μ	Dynamic viscosity (kg/m s)
γ	Ratio of specific heats (c_p/c_v)
λ	Molecular mean free path (m)
ν	Kinematic viscosity (m^2/s)
σ_T	Energy accommodation coefficient
σ_v	Momentum accommodation coefficient

H. Shokouhmand · S. Bigham (✉) · R. Nasr Isfahani
Department of Mechanical Engineering,
University of Tehran, Tehran, Iran
e-mail: sajjadbigham@ut.ac.ir; sajjadbigham@gmail.com

θ Dimensionless temperature
ξ Curvilinear horizontal coordinate
η Curvilinear vertical coordinate
τ Shear stress

Subscripts

ave Mean value
w Surface conditions
i Inlet conditions
s Fluid property near the wall

Superscripts

C Contravariant velocities
tang Tangential direction
* Returns to dimensional parameters

1 Introduction

Micro-scale heat transfer has received much interest as the size of the devices decreases, such as in electronic equipments, heat exchangers, sensors and flow controls, reactors, power systems and microelectromechanical systems (MEMS). Flow in constricted channels occurs in many bio-fluid systems (blood vessels with stenoses) or fluidic devices (orifices, valves) and have wide applications in engineering. So an accurate and efficient analysis of hydrodynamic and thermal behavior of gaseous flows in constricted microchannels seems necessary. However, a few experimental investigations is available to give a clear understanding of convective heat transfer rates and hydrodynamic characteristics of gaseous microchannel flows in the slip regime. Therefore, adequate and accurate numerical prediction tools for flow physics are particularly important. Numerous numerical studies on the hydrodynamic and thermal characteristics of flow in microchannels have been conducted [1–4].

Based on the magnitude of Knudsen number ($Kn = \lambda/L^*$, ratio between the gas mean free path and the length scale) fluid flows exhibit different behaviors. Therefore, some classifications have been done. According to the magnitude of Knudsen number flows are divided into four regimes: continuum, slip, transition and free molecular flows. In microchannels due to the minute length scale, the Knudsen number gets a significant value and it determines the behavior of fluid flow. In this work, the slip regime is studied and the Knudsen number is in the range from 0.001 to 0.1. Different investigations on the microchannel heat transfer in this regime have been carried out [5–7]. In this regime, velocity slip and temperature jump occur at the wall surface and thereby, flow characteristics such as Nusselt number and $C_f Re$ are influenced. Theoretical and numerical studies within the slip flow regime typically use the Navier–Stokes approach model and energy equation along with appropriate slip wall and temperature jump models.

Due to the wide application of constricted channels in industrial systems, various analytical and numerical works have been conducted for macro scale channels. For instance, Dennis and Smith [8] obtained numerical solution for a constricted channel problem with a Newtonian fluid for a wide range of Reynolds numbers by using a finite difference method. Vradis et al. [9] studied the steady, two-dimensional case in channel in curvilinear orthogonal and nonorthogonal coordinate systems. They illustrated that the vorticity remains constant in the straight section of the channel close to the inlet, increasing rapidly as the wall starts converging. Also it was shown that the vorticity peaks at the point where the cross-sectional area becomes minimum and drops rapidly as the flow enters the diverging part of the channel. Wang et al. [10] numerically studied forced convection in a symmetric wavy wall macro channel. Their results showed that the amplitudes of the Nusselt number and the skin-friction coefficient increase with an increase in the Reynolds number and the amplitude–wavelength ratio. The heat transfer enhancement is not significant at smaller amplitude wavelength ratio; however, at a sufficiently larger value of amplitude wavelength ratio the corrugated channel will be seen to be an effective heat transfer device, especially at higher Reynolds numbers. Cheng [11] studied a family of locally constricted channels and in each case, the shear stress at the wall was found to be sharply increased at and near the region of constriction. Due to wide application of constricted channels in the cardio vascular system, a large number of investigations (experimental and numerical computations) have been conducted on the flow disturbances caused by a locally single stenosis, e.g., Deshpande et al. [12], Ahmed and Giddens [13] and others.

Also in microscale gas flows, various analytical and numerical works have been conducted. Arkilic et al. [14] investigated helium flow through microchannels. It is found that the pressure drop over the channel length was less than the continuum flow results. The friction coefficient was only about 40% of the theoretical values. Also they noticed that the mass flow rate was increased compared with no-slip model prediction, which implied that the friction resistance was reduced. Harley et al. [15] presented an experimental and theoretical investigation of low Reynolds number, high subsonic Mach number, compressible gas flow in channels. The Knudsen number ranged from 0.001 to 0.4. Their simulation indicated that the pressure may be assumed to be uniform in the conduit cross-sections perpendicular to the direction of the flow and that the transverse velocity can be neglected. Beskok et al. [16] studied the rarefaction and compressibility

effects in gas microflows in the slip flow regime and for the Knudsen number below 0.3. Their formulation is based on the classical Maxwell-Smoluchowski boundary conditions that allow partial slip at the wall. It was shown that rarefaction negates compressibility. They also suggested specific pressure distribution and mass flow rate measurements in microchannels of various cross sections. Chen et al. [17] investigated the mixing characteristics of flow through microchannels with wavy surfaces. However, they modeled the wavy surface as a series of rectangular steps that it seems to cause computational errors at boundary especially in micro-scale geometry. Also their working fluid was liquid and they imposed no-slip boundary conditions at the microchannel wall surface.

The summary above shows that the hydrodynamic and thermal aspects of fluid flow in normal microchannels have already been studied. But, according to the authors' knowledge there is no study of hydrodynamic and thermal characteristics of fluid flow in constricted microchannels especially with slip boundary conditions. The present work is an attempt to fill the literature gap in this regard. The present work analyzes both the hydrodynamic and thermal aspects of a gaseous flow in the constricted microchannels.

2 Formulation of the problem

To begin with, Fig. 1 shows the geometry of interest which is seen to be a two-dimensional symmetric constricted channel. The channel walls are assumed to extend to infinity in the z-direction (i.e., perpendicular to the plane). The mathematical nondimensional expression of constricted wall is given as

$$y_w(x) = 0.5 - a\left(1 - \cos\left(2\pi\left(\frac{x}{\lambda} - 0.125\right)\right)\right) \tag{1}$$

Steady laminar flow with constant properties is considered. The present work is concerned with both thermally and hydrodynamically developing flow cases. In this study the usual continuum approach is coupled with two main characteristics of the micro-scale phenomena, the velocity slip and the temperature jump. A general non-orthogonal curvilinear coordinate framework with (ξ, η) as independent variables is used to formulate the problem. The non-dimensional governing equations can be written as:

Continuity:

$$\frac{\partial U^C}{\partial \xi} + \frac{\partial V^C}{\partial \eta} = 0 \tag{2}$$

X-momentum:

$$\begin{aligned}\frac{\partial}{\partial \xi}(uU^C) + \frac{\partial}{\partial \eta}(uV^C) = \frac{1}{Re_i}\Bigg\{&\frac{\partial}{\partial \xi}\left(q_{11}\frac{\partial u}{\partial \xi}\right) + \frac{\partial}{\partial \eta}\left(q_{22}\frac{\partial u}{\partial \eta}\right)\\ &+ \frac{\partial}{\partial \xi}\left(q_{12}\frac{\partial u}{\partial \eta}\right) + \frac{\partial}{\partial \eta}\left(q_{12}\frac{\partial u}{\partial \xi}\right)\Bigg\}\\ &- \frac{\partial}{\partial \xi}(y_\eta p) + \frac{\partial}{\partial \eta}(y_\xi p)\end{aligned} \tag{3}$$

Y-momentum:

$$\begin{aligned}\frac{\partial}{\partial \xi}(vU^C) + \frac{\partial}{\partial \eta}(vV^C) = \frac{1}{Re_i}\Bigg\{&\frac{\partial}{\partial \xi}q_{11}\frac{\partial v}{\partial \xi}\Bigg) + \frac{\partial}{\partial \eta}\left(q_{22}\frac{\partial v}{\partial \eta}\right)\\ &+ \frac{\partial}{\partial \xi}\left(q_{12}\frac{\partial v}{\partial \eta}\right) + \frac{\partial}{\partial \eta}\left(q_{12}\frac{\partial v}{\partial \xi}\right)\Bigg\}\\ &+ \frac{\partial}{\partial \xi}(x_\eta p) - \frac{\partial}{\partial \eta}(x_\xi p)\end{aligned} \tag{4}$$

Energy:

$$\begin{aligned}\frac{\partial}{\partial \xi}(\theta U^C) + \frac{\partial}{\partial \eta}(\theta V^C) = \frac{1}{Pe_i}\Bigg\{&\frac{\partial}{\partial \xi}\left(q_{11}\frac{\partial \theta}{\partial \xi}\right) + \frac{\partial}{\partial \eta}\left(q_{22}\frac{\partial \theta}{\partial \eta}\right)\\ &+ \frac{\partial}{\partial \xi}\left(q_{12}\frac{\partial \theta}{\partial \eta}\right) + \frac{\partial}{\partial \eta}\left(q_{12}\frac{\partial \theta}{\partial \xi}\right)\Bigg\}\end{aligned} \tag{5}$$

where:

$$U^C = uy_\eta - vx_\eta, \quad V^C = -uy_\xi + vx_\xi$$

$$J = x_\xi y_\eta - x_\eta y_\xi, \quad q_{11} = \frac{1}{J}(y_\eta^2 + x_\eta^2)$$

$$q_{12} = \frac{-1}{J}(x_\xi x_\eta + y_\xi y_\eta), \quad q_{22} = \frac{1}{J}(x_\xi^2 + y_\xi^2)$$

u, v are the physical velocity components and U^c and V^c are the velocities in ξ, η coordinates, respectively. Here, θ represents nondimensional temperature. The employed dimensionless variables are defined as follows:

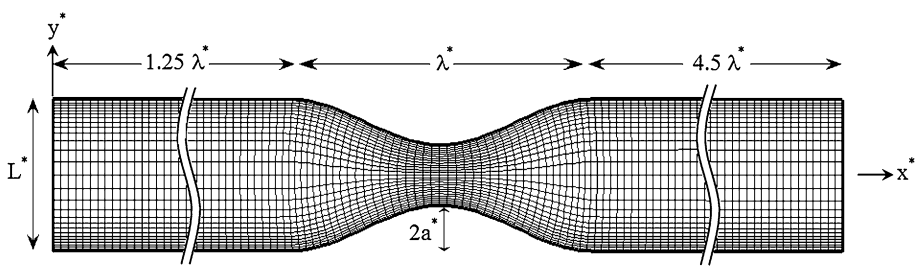

Fig. 1 Physical domain of constricted microchannel

$$x = \frac{x^*}{L^*}, \quad y = \frac{y^*}{L^*}, \quad p = \frac{p^*}{\rho u_i^{*2}}, \quad u = \frac{u^*}{u_i^*}$$

$$v = \frac{v^*}{u_i^*}, \quad Re_i = \frac{\rho u_i^* L*}{\mu}, \quad Pe_i = Re_i \,\mathrm{Pr} = \frac{u_i^* L^*}{\alpha}$$

$$\theta = \frac{T - T_i}{T_w - T_i}$$

Here, u_i^* and T_i are the inlet velocity and inlet temperature, respectively.

3 Slip flow effects and boundary conditions

Classical continuum physics cannot model a gaseous flow at low pressure or in a very small passage. A micro scale flow exhibits a nonzero flow velocity at solid boundaries and a nonzero difference between temperature of flow near solid boundaries and solid boundaries. It means at solid boundaries a slip flow and a temperature jump will be present. In order to estimate the slip effect at wall under rarified condition, the Maxwell slip condition has been widely used which is based on the first-order approximation of wall-gas interaction from kinetic theory of gases [18, 19]. The magnitude of tangential accommodation coefficient expresses the degree of non-elastic diffusive reflection between gas molecules and wall molecules [20]. Using von-Smoluchowski model we have the following boundary conditions at wall in curvilinear coordinate form:

$$U_s = \frac{2 - \sigma_v}{\sigma_v} Kn_i \left.\frac{\partial U_s}{\partial n}\right|_w + \frac{3}{2\pi}\frac{(1-\gamma)}{\gamma}\frac{Kn_i^2 Re_i}{Ec_i}\left.\frac{\partial \theta}{\partial s}\right|_w \tag{6}$$

$$\theta_s = 1 - \left(\frac{2 - \sigma_T}{\sigma_T}\right)\left(\frac{2\gamma}{\gamma + 1}\right)\frac{Kn_i}{\mathrm{Pr}_i}\left.\frac{\partial \theta}{\partial n}\right|_w$$

where γ and σ represent the specific heat ratio and accommodation coefficient, respectively. The second term in the slip velocity associates with the thermal creep. The thermal creep (transpiration) phenomenon is a rarefaction effect. It shows that even without any pressure gradient the flow can be caused due to tangential temperature gradient, specifically from colder region toward warmer region. Thermal creep effects can be important in causing variation of pressure along microchannels in the presence of tangential temperature gradients. The creeping flow affects Nusselt number in two opposite directions. One of them is when creep flow in the same direction as the mean flow increases the total slip velocity, which increases the energy exchange near the wall and tends to increase *Nu*. While in the other way, creep flow in the opposite direction of the mean flow decreases the total slip velocity, which decreases the energy exchange near the wall and tends to decrease *Nu* [21–23].

Here, Ec_i means the Eckert number which is defined as

$$Ec_i = \frac{u_i^{*2}}{c_p(T_w - T_i)} \tag{7}$$

where, *Pr* and *Kn* mean the Prandtl number and Knudsen number, respectively. The Knudsen number shows the effect of rarefaction on flow properties. A nonzero Knudsen number means a slip flow with nonzero flow velocity at the boundaries and nonzero temperature difference between the boundaries and adjacent flow. In the present work, the slip flow regime with the Knudsen number ranging from 0.01 to 0.1 is considered.

In this work, the study is limited to incompressible flow. The flow can be considered incompressible for Mach number lower than 0.3 [22]. In order to keep the Mach number below 0.3, the upper limit of *Re* should be determined. The following equation relating Mach number, Knudsen number and Reynolds number was suggested by Morini et al. [24] in microchannel flow.

$$Re = \frac{Ma}{Kn}\sqrt{\frac{\pi\gamma}{2}} \tag{8}$$

By referring to Eq. (8) and the range of *Kn* considered in this work, the flow will be incompressible with $Re = 2$. Hence, all subsequent results presented were obtained using this Reynolds number.

The wall temperature is set at a constant temperature T_w, which is higher than the gas flow inlet temperature T_i. The nondimensional wall temperature is set at unity.

Moreover, the other boundary conditions should be defined. A uniform inlet velocity and temperature are specified as

$$u = 1, \quad v = 0, \quad \theta = 0 \tag{9}$$

In the outlet, fully developed boundary conditions are assumed as

$$\frac{\partial u}{\partial x} = \frac{\partial v}{\partial x} = \frac{\partial \theta}{\partial x} = 0 \tag{10}$$

4 Calculations for Nusselt number and $C_f Re$

Friction coefficient for a hydrodynamically-thermally developing flow in the microchannel is calculated by,

$$C_f = \frac{\tau_w^*(x)}{\rho\left(u_{\mathrm{ave}}^*(x)\right)^2} \tag{11}$$

where $u^*_{\mathrm{ave}}(x)$ represents the average velocity and $\tau^*_w(x)$ is the wall shear stress defined as

$$\tau_w^* = \mu\frac{\partial u^{*\tan g}(x)}{\partial n^*} \tag{12}$$

Moreover, the average velocity can be expressed in nondimensional form as

$$u_{\text{ave}}(x) = \frac{1}{2y_w(x)} \int u(x,y)\mathrm{d}y \tag{13}$$

where y(x) represents the half width of microchannel. Combining Eqs. 11–13 gives

$$C_f Re = \frac{4(y_w(x))^2}{\left(\int u(x,y)\mathrm{d}y^2\right)} \frac{\partial u^{\tan g}(x)}{\partial n} \tag{14}$$

The local *Nu* Number is calculated by

$$Nu = \frac{hL^*}{k} \tag{15}$$

In addition, the heat wall flux is defined as

$$q'' = h(T_w - T_{\text{ave}}) \tag{16}$$

The heat flux may also be expressed in term of tangential temperature gradient at wall as

$$q'' = -k \frac{\partial T}{\partial n^*}\bigg|_w \tag{17}$$

Combining Eqs. 15–17 in nondimensional form result in Nusselt number as

$$Nu = \frac{1}{\theta_{\text{ave}}(x) - 1} \frac{\partial \theta(x)}{\partial n}\bigg|_w \tag{18}$$

5 Validation of numerical code

In Fig. 2a, a comparison with the previously published result of Wang and Chen [10] is carried out to validate the numerical code and non-orthogonal grid discretization scheme of the present study. Their model is analogous to the present model but with the water as working fluid and macro scale channel. Also there is no slip effect with fixing *Kn* number at zero.

To investigate the accuracy of the used numerical model for the special case of microchannel, the obtained numerical results for slip flow are compared with analytical results of microchannel in [25]. The used parameters in [25] for nondimensional temperature and Nusselt number can be shown in terms of this work as follows:

$$\theta = 1 + 6Ec_i \,\mathrm{Pr}\left(1 - \frac{u_s}{u_m}\right)\left[3(1-y)^2 y^2 + \frac{u_s}{u_m}\left\{\left(y - y^2\right)\left[1 - 3\left(y - y^2\right)\right] + 2\beta_T Kn\right\}\right] \tag{19}$$

$$Nu_\infty = 420\frac{u_s}{u_m}\left[27 + (9 + 420\beta_t Kn)\frac{u_s}{u_m} - \left(\frac{u_s}{u_m}\right)^2\right]^{-1} \tag{20}$$

which

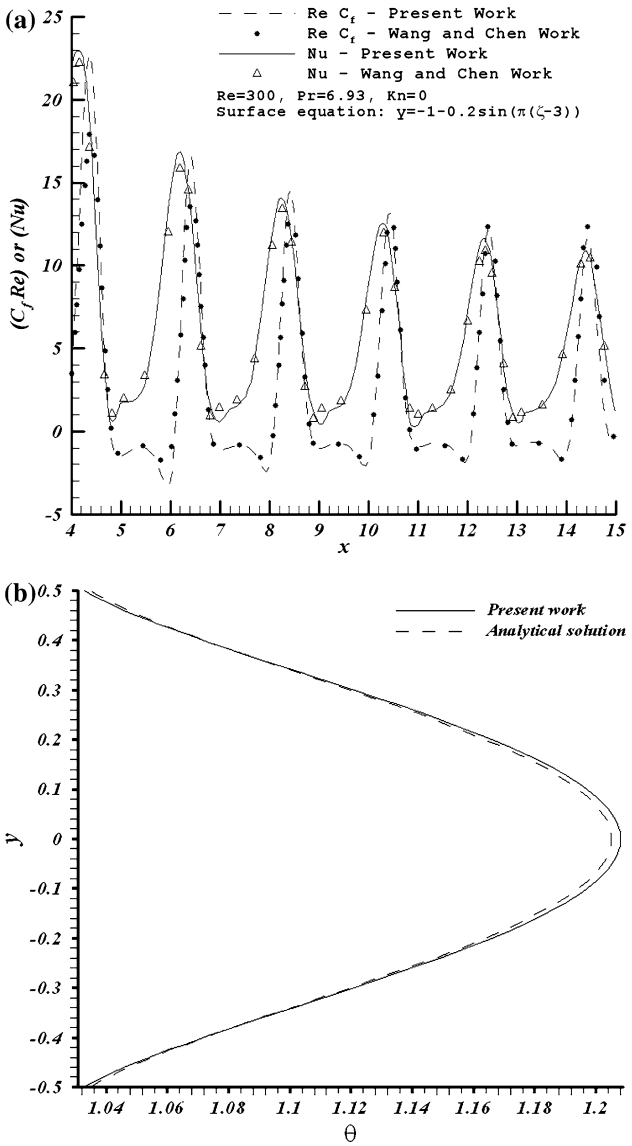

Fig. 2 **a** Validation of the numerical code with available results. **b** Validation of the numerical code with available results

$$\beta_v = \frac{2 - \sigma_v}{\sigma_v}, \quad \beta_T = \frac{2 - \sigma_T}{\sigma_T}\frac{2\gamma}{1+\gamma}\frac{1}{\mathrm{Pr}}$$

This comparison is carried out for the $Kn = 0.04$, $Pr = 0.7$, $Pe = 0.5$, $Ec = 0.286$, $\beta_v = 1$ and $\beta_T = 1.667$. In the numerical code, two dimensional forms are considered for the convective and diffusive terms. To compare the analytical and numerical solutions, the viscous dissipation term in the analytical solution is also added to the numerical solution. Also the flow work term in the analytical solution is considered in the numerical model. The analytical solution results 3.47 for the Nusselt number, while the numerical model gives 3.53 for the fully developed Nusselt number which are in a good agreement. Furthermore, the nondimensional temperature profiles for the

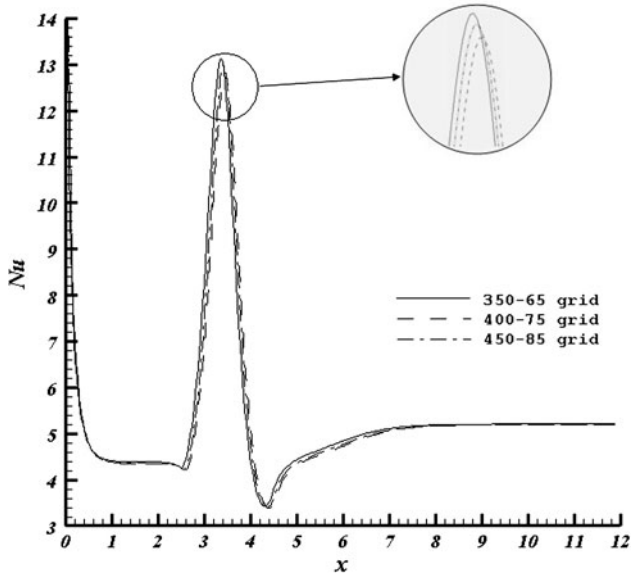

Fig. 3 Numerical results of local Nusselt number along the constricted microchannel with $Kn = 0.075$ at $Re = 2$ and $a = 0.15$

two models are shown in Fig. 2b which are also in a good agreement.

6 Grid independency

The resulting numerical velocity and temperature fields may be used to calculate $C_f Re$ and Nu along the length of the microchannel. The accuracy of the numerical solutions and the time required to reach a solution are dependent on the grid resolution. In this paper, all computations are performed on three grids comprising 350 × 65, 400 × 75 and 450 × 85 control volumes respectively. The obtained results showed sufficient accuracy on these range of grid resolutions. For instance, this accuracy is indicated for Nu along the microchannel with the conditions specified in Fig. 3. Grid dependence studies have been completed with similar results for each numerical solution presented in the results section. Hence, for simplicity all subsequent results presented in result section are obtained using 400 × 75 grid.

7 Solution procedure

The governing equations with appropriate boundary conditions are solved by employing the SIMPLE algorithm [26], a finite volume method, in non-orthogonal curvilinear coordinate framework. The HYBRID differencing [27] is applied for the approximation of the convective terms. The Poisson equations is solved for (x, y) to find grid points [28] and are distributed in a nonuniform manner with higher concentration of grids close to the curvy walls and normal to all walls, as shown in Fig. 1. In this work, a full-staggered grid is used. In this type of grid, scalar variables such as pressure and temperature at ordinary points are evaluated but velocity components are calculated around the cell faces. Also the control volumes for u and v are different from the scalar control volumes and different from each other. The discrete form of the momentum and energy equations and all the boundary conditions are obtained by applying a second order central difference scheme. While for boundary nodal points, the one-way difference scheme is applied (i.e., forward for lower and inlet boundaries and backward for upper and outlet boundaries).

In the numerical procedure of this paper, first the velocity and temperature fields are guessed. The macro scale channel boundary conditions are applied as the initial microchannel boundary conditions. Then the velocity components are obtained by solving the momentum equations with the mentioned initial boundary conditions. With this new velocity field, one can solve the energy equation with initial temperature boundary conditions to find the temperature field. Now the slip velocity and the temperature jump which are used to correct boundary conditions are obtained from Eq. 6. Then the above algorithm is repeated till the convergence criteria are satisfied. With the resulted velocity and temperature fields, the thermal and hydrodynamic characteristics of the flow in the microchannel such as Nusselt number and friction factor, which are the two major subjects of studies in the microchannels, can be obtained. One convergence criteria is a mass flux residual less than 10^{-8} for each control volume. Another criteria that is established for the steady state flow is $(|\varphi_{i+1}-\varphi_i|)/|\varphi_{i+1}| \leq 10^{-10}$ where φ represents any dependent variable, namely u, v and θ, and i is the number of iteration.

8 Results and discussion

The mathematical model developed in the previous sections is applied to predict the fluid flow and heat transfer characteristics (i.e., the velocity field, local temperature field, friction factor and local Nusselt number) through the constricted microchannel. To reduce the computation work, only one half of microchannel, shown in Fig. 1, is considered due to the symmetrical conditions. However, the results presented in the results section are shown for the whole microchannel. In this work, the effects of Knudsen number, Reynolds number and geometry on fluid flow and heat transfer characteristics of constricted microchannel is numerically simulated. The boundaries are maintained at temperature $T_w = 70°C$ and the uniform inlet temperature is considered $T_i = 25°C$. The tangential momentum

Table 1 Numerical values for Ec as a function of Kn at $Re = 2$

	$Kn = 0.01$	$Kn = 0.025$	$Kn = 0.05$	$Kn = 0.075$	$Kn = 0.1$
Ec	4.82×10^{-4}	3.01×10^{-3}	1.21×10^{-2}	2.71×10^{-2}	4.82×10^{-2}

accommodation coefficient σ_v and the thermal accommodation coefficient σ_T are set at 0.9. The results are obtained for the specific heat ratio $\gamma = 1.4$ and $\Pr = 0.7$. Also geometry parameters is taken $\lambda = 2$.

In the numerical code, the Ec number is not treated as a constant and independent variable, but the Ec number is calculated with the wall and inlet temperatures which are taken constant and the given Re and Kn numbers. For the Ec number to be calculated, the inlet velocity is also needed. In order to find the inlet velocity, the Re and Kn are used with Eq. 8 to have the Ma Number. Then the Inlet velocity is simply calculated with Eq. 21. Finally, the Ec number which is needed in the numerical procedure is found using Eq. 7. As stated above, in the numerical code, the Ma number is not necessary and it is only used to calculate the needed Ec number.

$$u_i^* = Ma\sqrt{\gamma RT_i} \tag{21}$$

The data on Table 1 shows the five studied Knudsen numbers and corresponding Eckert numbers.

8.1 The flow field

Figure 4 displays the effect of Kn on slip velocity for hydrodynamically/thermally developing flow in the constricted microchannel. By increasing the Knudsen number, the channel dimensions decrease and approach to molecular dimensions. By decreasing the microchannel dimensions, the MFP (mean free path) becomes more comparable with the microchannel's characteristic length in size. This means that the thickness of Knudsen layer increases that causes an increase in the slip velocity. Furthermore, decreasing the microchannel dimensions lead to a decline in the interaction of gaseous molecules with the adjacent walls. Therefore, the momentum exchange between the fluid and adjacent walls reduces. This reduction means that the fluid molecules are lesser affected by the walls that leads to larger slip velocity. Moreover, in the convergent region, the cross section area decreases that causes the acceleration of the fluid flow. So the average velocity increases that contributes to a rapid raise in the slip velocity in this region.

As shown in Figs. 5 and 6, the velocity profiles in two different locations in the constricted region are plotted. It is observed that by increasing the rarefaction, the slip flow is intensified. Clearly, the figure demonstrates that the velocity at the boundary is not equal to zero, and that the

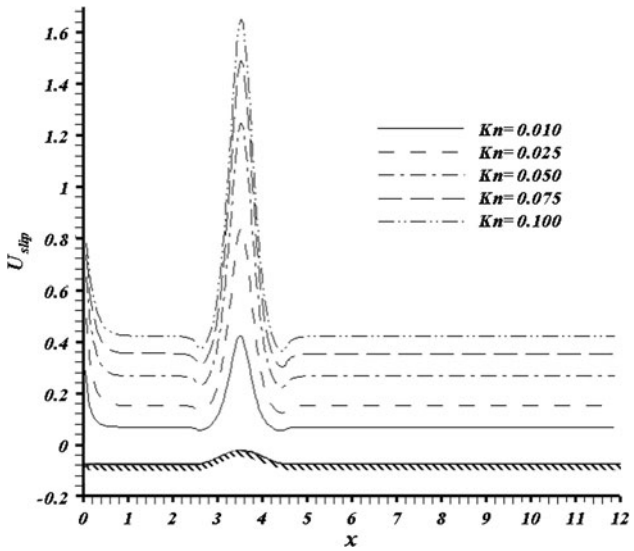

Fig. 4 Variation of slip velocity along the constricted microchannel with Knudsen number $Re = 2$ and $a = 0.15$

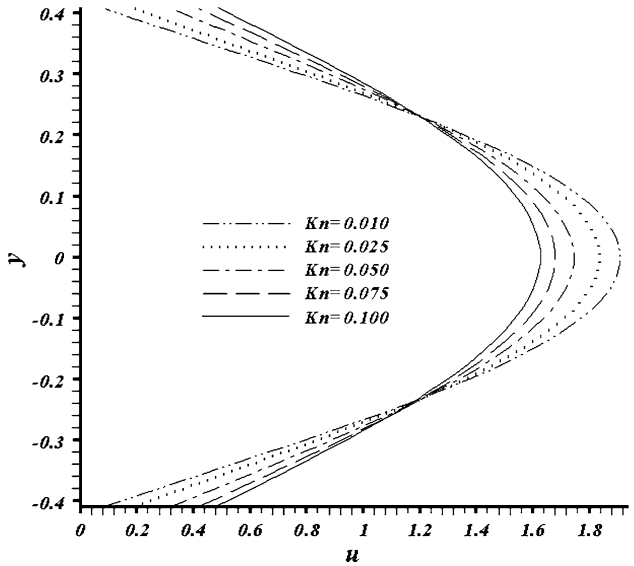

Fig. 5 Variation of velocity profile at $x = 1.5\lambda$ in the constricted microchannel with Knudsen at $Re = 2$ and $a = 0.15$

velocity is dependent upon the Knudsen value. As illustrated in these two figures, when the slip velocity increases, the velocity profile gets flatter that leads to the reduction in wall velocity gradients.

Moreover, the locations of these two figures are chosen intentionally with the same distances before and after the throttle area (i.e., $x = 1.5, 2\lambda$) to find the effect of divergency and convergency on the velocity profile. As it is shown, the divergency or convergency of channel does not affect the velocity profiles. In other words, the size of cross section area determines the velocity profile in this laminar flow regime.

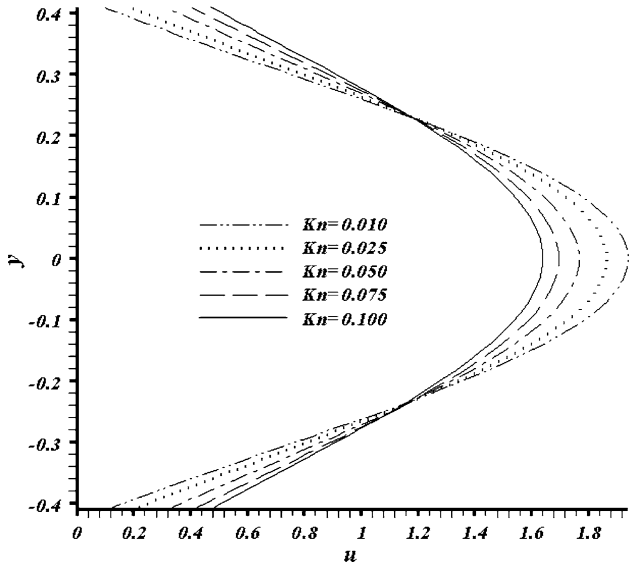

Fig. 6 Variation of velocity profile at $x = 2\lambda$ in the constricted microchannel with $Re = 2$ and $a = 0.15$

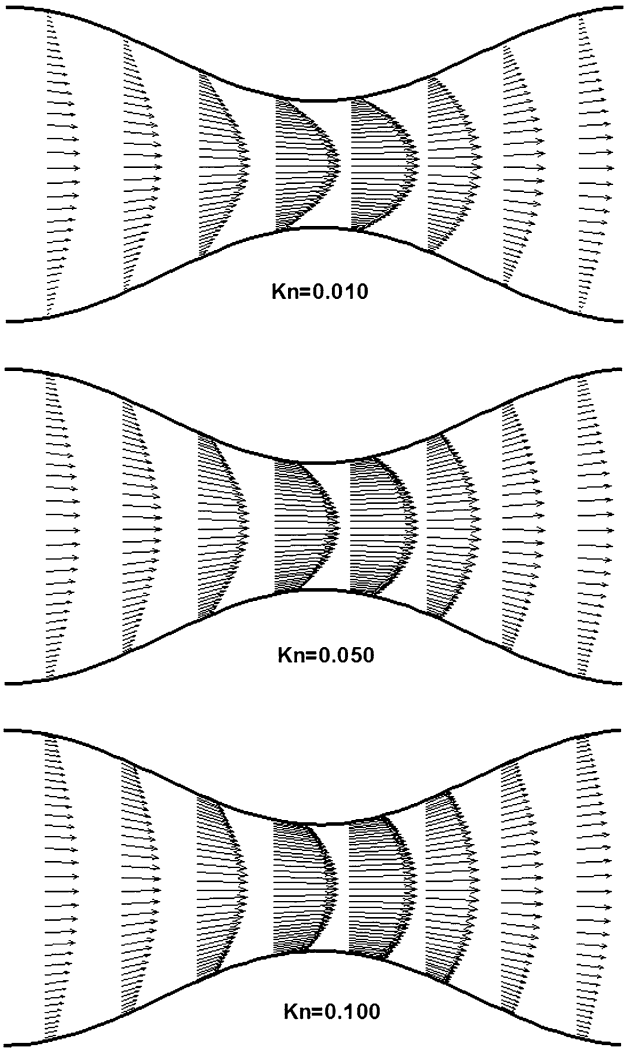

Fig. 7 Schematic illustration of Knudsen number effect on velocity profile at $Re = 2$ and $a = 0.15$

Figure 7 schematically illustrates the effect of rarefaction on velocity profile in different cross sections. This figure gives a clear understanding of the increasing effect of Knudsen number on slip velocity. In addition, in each Knudsen number as the fluid approaches the throttle region, the slip velocity becomes more considerable.

Figure 8 depicts the effect of Knudsen number on $C_f\,Re$ for hydrodynamically/thermally developing flow in the constricted microchannel. It is evident that there is high friction at the entrance region due to presence of high velocity gradients. However, it rapidly decreases as the flow develops. Furthermore, Knudsen has a decreasing effect on the friction factor. This effect can be explained physically. By increasing the Knudsen number, as already stated, the interaction of gaseous molecules with the adjacent walls decreases. Therefore, the momentum exchange between the fluid and adjacent walls reduces and this means $C_f\ Re$ declines. Furthermore, as rarefaction increases, the slip velocity increases which results in a flatter velocity profile with reduced wall velocity gradients that contributes to the decrease in $C_f\,Re$. Also this effect can be explained by referring to the definition of $C_f\ Re$. Equation 14 shows that $C_f\ Re$ depends on the average velocity and the gradient of tangential velocity. As Knudsen increases, due to a fixed Re and Eq. 8 we have higher Mach number that results in greater average velocity. In addition, in according to Fig. 5, larger Knudsen number decreases the slop of velocity near the wall and this means having lesser tangential velocity gradient. Therefore, in according to the previous explanation, the larger Knudsen number causes the lesser $C_f\,Re$. Moreover, by variation of Knudsen number from 0.01 to 0.1, the $C_f\,Re$ at the end of microchannels decreases 38%.

Besides, as shown in Fig. 8, $C_f\,Re$ experiences a rapid decrease in the convergent region in the microchannel. To explain this phenomenon, one should refer to the definition of $C_f\,Re$ in Eq. 14. In this equation, there are two different parameters that should be considered separately. The first parameter is the gradient of tangential velocity, $\partial u^{\text{tang}}(x)/\partial n$ and second parameter is the ratio shown below.

$$\frac{4(y_w(x))^2}{\left(\int u(x,y)\mathrm{d}y\right)^2} \tag{22}$$

To explain the effect of these two parameters, they are plotted in Fig. 9 along the microchannel for the special case of $Kn = 0.1$. In order to clarify this comparison their logarithms are shown. Thus, the sum of them results in the

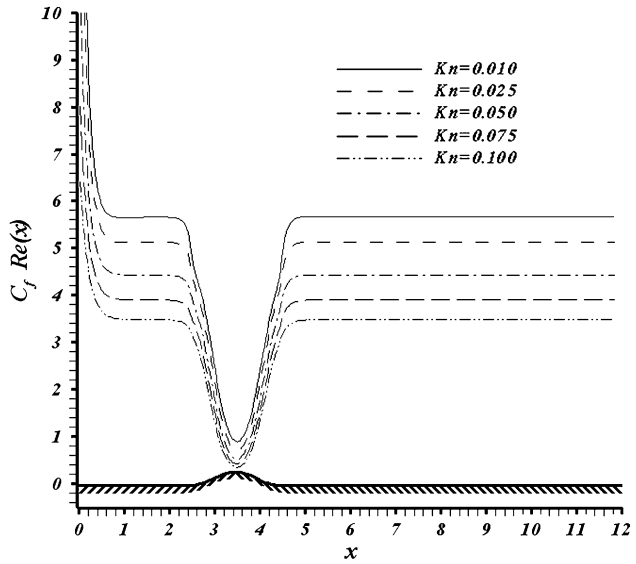

Fig. 8 Variation of $C_f\,Re$ along the constricted microchannel with Knudsen number at $Re = 2$ and $a = 0.15$

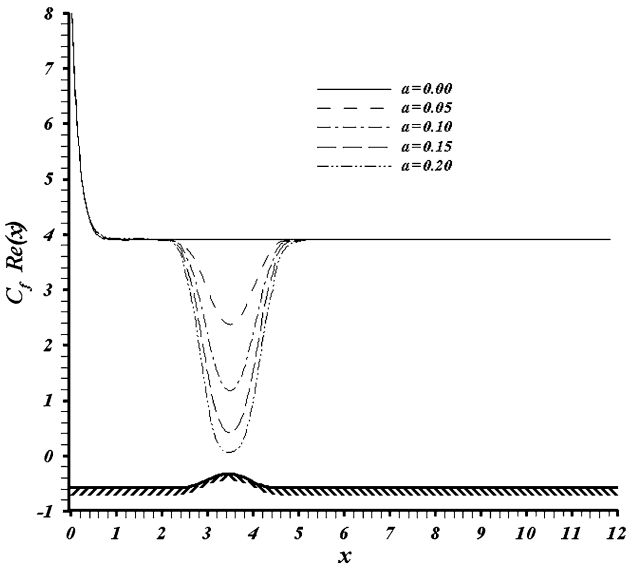

Fig. 10 Variation of $C_f\,Re$ along the constricted microchannel with geometry at $Re = 2$ and $Kn = 0.075$

logarithm of $C_f\,Re$. As it can be seen, these two parameters show different behavior in the convergent part. As expected, the gradient of tangential velocity increases in the convergent region. While the parameter shown in Eq. 22 declines rapidly due to the decrease of channel width, $y_w(x)$ and the growth of average velocity, $\int u(x,y)\mathrm{d}y$. Therefore, more attention should be paid to the intensity of variations of these two parameters. As depicted, intensity of variation of the second parameter is more significant. So in this case, the second term is dominant and determines the behavior of $C_f\,Re$.

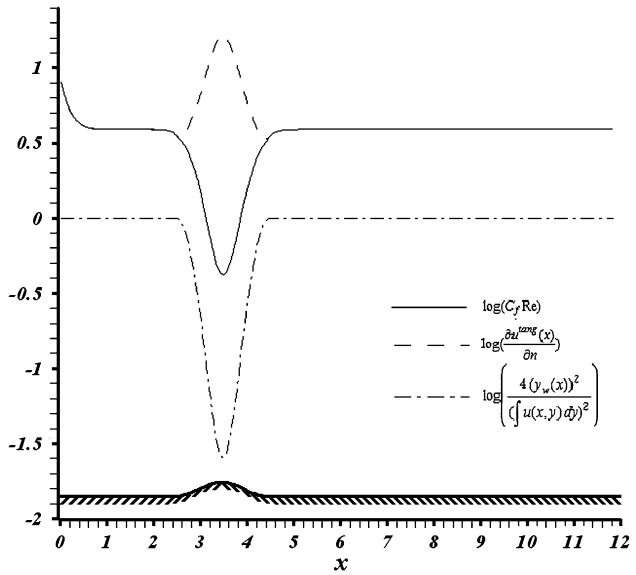

Fig. 9 Variation of $C_f\,Re$ along the constricted microchannel at $Re = 2$, $Kn = 0.075$ and $a = 0.15$

Figure 10 displays the effect of throttle area on $C_f\,Re$ while keeping the Reynolds number and Knudsen number constant. By decreasing the throttle area (i.e., increasing the constriction), the effect of constriction on the fluid flow is more noticeable. As it can be seen by decreasing the throttle area and subsequently the more increase in the average velocity, $C_f\,Re$ experiences more intense decrease in the convergent region. For instance, $C_f\,Re$ decreases up to 5% in $a = 0.05$ in the constriction region, while this decrease is up to 57% in $a = 0.2$.

8.2 The temperature field

The effect of Knudsen number on temperature jump is depicted in Fig. 11. As shown, larger Knudsen numbers, higher temperature jumps. By decreasing of the channel dimensions, the thickness of the Knudsen number layer increases that bring about further temperature jump. In addition, it is found that this effect is gradually diminishing as the fluid flow approaches the developed region.

Figure 12 illustrates the variation of average temperature versus the length of microchannel for different Knudsen numbers. Intensification of the rarefaction results in augmenting the temperature jump at solid boundary. It means the nondimensional fluid temperature near the wall approaches the inlet nondimensional temperature that causes the decrease of average nondimensional temperature.

In addition, by considering a fixed Re and referring to Eq. 8, the larger Knudsen number brings about higher Mach number and this means the larger inlet velocity and momentum of fluid. As the fluid enters with greater

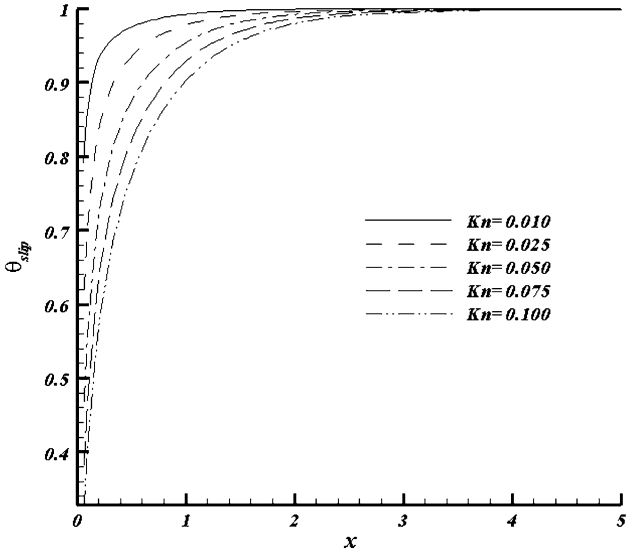

Fig. 11 Variation of the fluid temperature near the wall with Knudsen number along the constricted microchannel at $Re = 2$ and $a = 0.15$

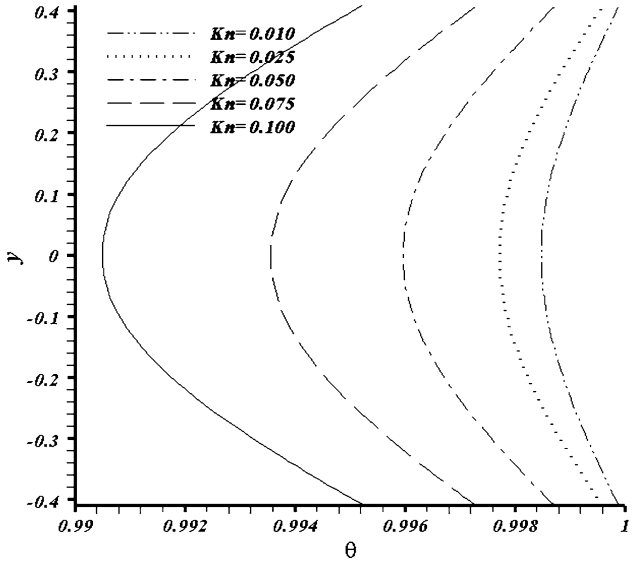

Fig. 13 Variation of temperature profile at $x = 1.5\lambda$ in the constricted microchannel with Knudsen at $Re = 2$ and $a = 0.15$

momentum, it loses its chance to exchange energy with the adjacent walls. This means the fluid needs longer distance to develop thermally.

Temperature distribution in two different cross sections at $x = 1.5, 2\lambda$ are given in Figs. 13 and 14. As expected with larger Knudsen number, we have higher temperature jump at the wall. In according to the definition, a unity nondimensional temperature means the temperature of the fluid equals wall temperature. Intensification of Knudsen number causes the center nondimensional temperature to approach the inlet nondimensional temperature more. In addition the temperature jump is more considerable in convergent region (i.e., Fig. 13) for low and high Knudsen numbers. It can be noticed that the wall temperature gradients are negative at the lower wall. Also, its absolute value is intensified by increasing the Knudsen number.

The effect of Knudsen number on local Nusselt number for hydrodynamically/thermally developing flow in the constricted microchannel is presented in Fig. 15. As expected, very high heat transfer rate is experienced in the entrance region of the microchannel due to high temperature gradient. As expected also, high heat transfer rate

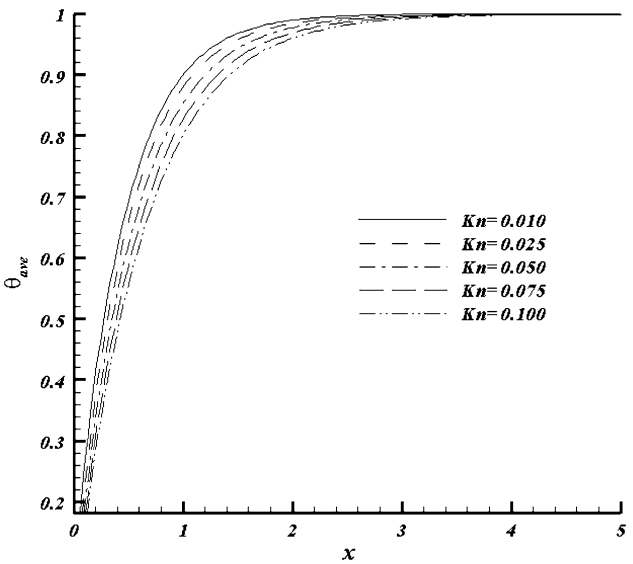

Fig. 12 Variation of average velocity with Knudsen number along the constricted microchannel with $Re = 2$ and $a = 0.15$

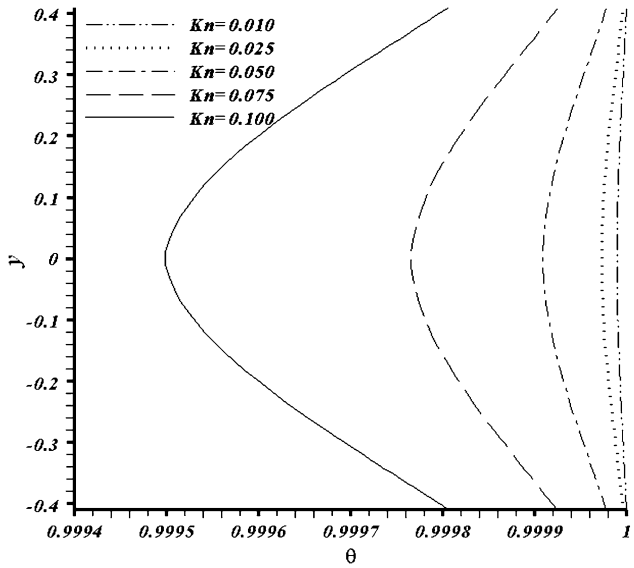

Fig. 14 Variation of temperature profile at x=2λ in the constricted microchannel with Knudsen at $Re = 2$ and $a = 0.15$

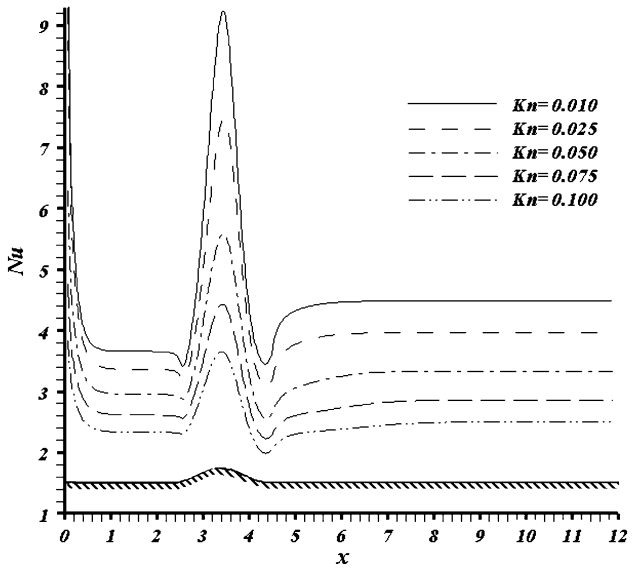

Fig. 15 Variation of local Nusselt number along the constricted microchannel with Knudsen at $Re = 2$ and $a = 0.15$

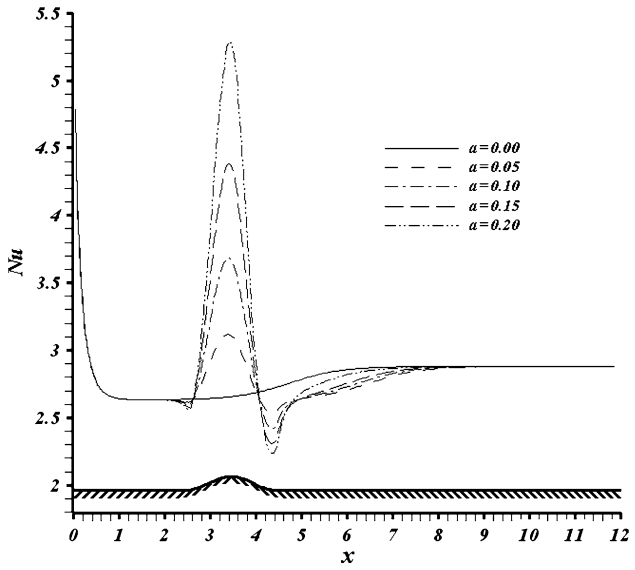

Fig. 16 Variation of local Nusselt number along the constricted microchannel with amplitude at $Kn = 0.075$ and $Re = 2$

diminishes rapidly as the thermally developing flow approaches the fully developed flow.

Due to the increasing of the average velocity and especially slip velocity in the convergent region, there is a jump in the local Nusselt in this region. For instance, in the constriction region for $Kn = 0.01$, the Nusselt increases up to 153%. While this enhancement in heat transfer rate is lesser for larger Knudsen number, e.g. 56% for $Kn = 0.1$. There is a same phenomenon in macro scale channel because of larger average velocity in converging region. As mentioned above, in microchannel, slip velocity has a great jump in constricted region and this can amplifies the heat transfer coefficient. After this region and approaching the fully developed flow, local Nusselt converges to a constant value (i.e., there is no change in local Nusselt number). Moreover, it can be noticed that the Nusselt number even after the constriction does not return to its value before the constriction and has a greater value. It means that the constriction enhances the heat transfer rate.

Besides, Nusselt number in the microchannel lower as the rarefaction increases. As already sated, when rarefaction increases the temperature jump as well as slip velocity is intensified. Here, as temperature jumps, the average temperature approaches the inlet temperature. The temperature jump acts like a thermal contact resistance between the wall and gas. However, the slip velocity tends to decrease this thermal resistance. In other words, the effects of the temperature jump and slip velocity are opposite on Nusselt number. The slip velocity acts to increase the Nusselt number by increasing the fluid velocity near the wall. Contrary to the slip velocity, the temperature jump decreases the Nusselt number by increasing the difference of the wall temperature and mean fluid temperature. In this work, with $\sigma_v = 0.9$, $\sigma_T = 0.9$ and the specified constricted geometry, the effect of temperature jump in Nusselt number is more important.

In Fig. 16 the effect of variation of throttle area on Nusselt number while keeping the Reynolds number and Knudsen number constant is plotted. By increasing constriction the fluid flow senses the variation of cross section more. As it can be seen by decreasing the throttle area, Nusselt number experiences much larger jump in the convergent region due to increase in the average velocity. For instance, Nusselt number increases up to 18% in $a = 0.05$ in the constriction region, while this increase is up to 100% in $a = 0.2$.

In Fig. 17, the developed $C_f Re$ and Nusselt numbers at the end of constricted microchannel verses Knudsen number are reported. The decreasing effect of Knudsen number on developed Nusselt number and $C_f Re$ is obvious in this figure. Moreover, by variation of Knudsen number from 0.01 to 0.1, the $C_f Re_\infty$ and Nu_∞ declines 38 and 44%, respectively.

9 Conclusion

The flow and heat transfer characteristics of laminar incompressible gas flow in a constricted microchannel is numerically investigated. Continuity, momentum and energy equations with slip boundary conditions at the solid walls are solved by SIMPLE algorithm in curvilinear coordinate.

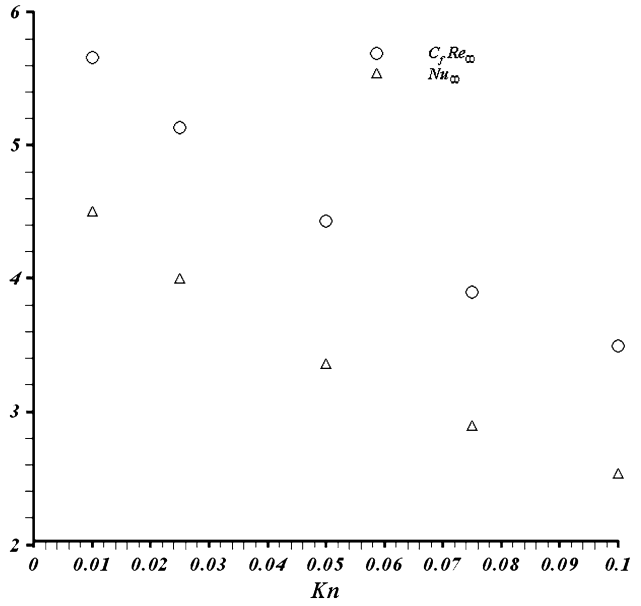

Fig. 17 Variation of developed $C_f\ Re$ and Nusselt numbers with Knudsen number at $Re = 2$ and $a = 0.15$

This paper investigates the effects of Knudsen number and geometry on thermal and hydrodynamic characteristics of flow in the constricted microchannel at constant Reynolds number. It is found that the Nusselt number and $C_f Re$ decrease with Knudsen number. It is also found that Nusselt number experiences a rapid jump in the convergent part and this jump is more considerable for lower Knudsen numbers. Furthermore, convergent region makes $C_f Re$ to decrease rapidly. The very high heat transfer rate and $C_f Re$ at the entrance declines rapidly as the thermally/hydraulically developing flow approaches fully developed flow. In addition, the model successfully predicts the growth of temperature jump and slip velocity with Knudsen number at the solid walls. Moreover, by decreasing the throttle area, the variation of Nusselt number and $C_f\ Re$ in the constricted region become more intense.

References

1. Galvis E, Jubran BA, Xi F, Behdinan K, Fawaz Z (2008) Numerical modeling of pin–fin micro heat exchangers. Heat Mass Transf 44:659–666
2. Graur IA, Méolans JG, Zeitoun DE (2006) Analytical and numerical description for isothermal gas flows in microchannels. Microfluid Nanofluid 2:64–67
3. Jiji LM (2008) Effect of rarefaction, dissipation, and accommodation coefficients on heat transfer in microcylindrical couette flow. ASME J Heat Transf 130:385–393
4. Jie D, Diao X, Cheong KB, Yong LK (2000) Navier–Stokes simulations of gas flow in micro devices. J Micromech Microeng 10:372–379
5. Chen CS, Kuo WJ (2004) Heat transfer characteristics of gaseous flow in long mini- and microtubes. Numer Heat Transf Part A Appl 46:497–514
6. Larrode FE, Housiadas C, Dreossinos Y (2000) Slip-flow heat transfer in circular tubes. Int J Heat and Mass Transf 43:2669–2680
7. Kavehpour HP, Faghri M, Asako Y (1997) Effects of compressibility and rarefaction on gaseous flows in microchannels. Numer Heat Transf Part A Appl 32:677–696
8. Dennis SCR, Smith FT (1980) Steady flow through a channel with a symmetrical constriction in the form of a step. Proc R Soc Loud A 372:393–414
9. Vradis G, Zalak V, Bentson J (1992) Simultaneous, variable solutions of the incompressible steady Navier-Stokes equations in general curvilinear coordinate systems. Trans ASME I J Fluids Engng 114:299–305
10. Wang CC, Chen CK (2004) Forced convection in a wavy-wall channel. Int J Heat Mass Transf 47:3877–3887
11. Cheng RT-S (1972) Numerical Solution of the Navier-Stokes Equations by the Finite Element Method. Phys Fluids 15:2098–2105
12. Deshpande MD, Giddens DP, Mabon RF (1976) Steady laminar flow through modelled vascular stenoses. J Biomech 9:165–174
13. Ahmed SA, Giddens DP (1983) Flow disturbance measurements through a constricted tube at moderate Reynolds number. J Biomech 16:955–963
14. Arkilic EB, Breuer KS, Schmidt MA (1994) Gaseous flow in microchannels. ASME Appl Microfabrication Fluid Mech 197:57–66
15. Harley JC, Huang Y, Bau HH, Zemel JN (1995) Gas flow in micro-channels. J Fluid Mech 284:257–274
16. Beskok A, Karniadakis GE, Trimmer W (1996) Rarefaction and compressibility effects in gas microflows. ASME J Fluids Eng 118:448–456
17. Chen CK, Cho CC (2007) Electro-kinetically-driven flow mixing in microchannels with wavy surface. J Colloid Interf Sci 312:470–480
18. Kennard EH (1938) Kinetic theory of gasses. McGraw-Hill, New York
19. Gombosi TI (1994) Gas kinetic theory. Cambridge University Press, New York
20. Gad-el-Hak M (2002) The MEMS Handbook, CRC Press LLC, Boca Raton
21. Karniadakis GE, Beskok A, Aluru N (2004) Micro flows and nanoflows fundamental and simulation. Springer, USA
22. Kandlikar S, Garimella S, Li D, Colin S, King MR (2006) Heat transfer and fluid flow in minichannels and microchannels, Elsevier, Britain
23. Liou WW, Fang Y (2006) Microfluid mechanics principal and modeling. McGraw-Hill, New York
24. Morini GL, Spiga M, Tartarini P (2004) The rarefaction effect on the friction factor of gas flow in microchannels. Superlattices and microstructures 35:587–599
25. van Rij J, Ameel T, Harman T (2009) The effect of viscous dissipation and rarefaction on rectangular microchannel convective heat transfer. Int J Therm Sci 48:271–281
26. Patankar SV (1972) A calculation procedure for heat, mass and momentum transfer in three-dimensional parabolic flows. Int J Heat Mass Transf 15:1787–1806
27. Spalding DB (1972) A novel finite difference formulation for differential expressions involving both first and second derivatives. Int J Numer Methods Eng 4:551–559
28. Hoffman KA (1989) Computational fluid dynamics for engineers. Eng Educ Sys, Austin